

Potential of Articulated Split Wingtips for Morphing-Based Control of a Flying Wing

P. Bourdin*, A. Gatto*, and M.I. Friswell†

University of Bristol, Bristol, England BS8 1TR, United Kingdom

This paper investigates a novel method for the control of ‘morphing’ aircraft. The concept consists of a pair of articulated split wingtips, independently actuated and mounted on a baseline flying wing. The general philosophy behind the concept was that adequate control of a flying wing about its three axes could be obtained through local modifications of the dihedral angle at the wingtips, thus providing an alternative to conventional control effectors such as elevons and drag rudders. Preliminary computations with a vortex lattice model and subsequent wind tunnel tests demonstrate the viability of the concept, with individual and/or combined wingtip deflections producing multi-axis, coupled control moments.

Nomenclature

b	wing span
C_l, C_m, C_n	rolling, pitching and yawing moment coefficients
C_{D_i}	lift-induced drag coefficient
C_{L_x}	lift coefficient derivative w.r.t. parameter x
$C_{l_x}, C_{m_x}, C_{n_x}$	rolling, pitching and yawing moment coefficient derivatives w.r.t. parameter x
D, C_D	drag, drag coefficient
g	gravitational acceleration
L, C_L	lift, lift coefficient
p, q, r	aircraft rotation rates in body or stability axes
R	turn radius
V_{cg}	flight speed
W	aircraft weight
CG	centre of gravity
LE	leading edge
TE	trailing edge
VLM	vortex lattice method
<i>Symbols</i>	
α	angle of attack
γ_{LA}, γ_{RA}	left and right aft wingtip dihedral angles
γ_{LF}, γ_{RF}	left and right fore wingtip dihedral angles
Ω	turn rate
ϕ	bank angle
ρ	air density

I. Introduction

SINCE the dawn of powered flight more than one hundred years ago, aircraft designers have sought to improve on existing aircraft control methodologies. In those early years, structural compliance techniques

*Research Associate, Dept. of Aerospace Engineering.

†Professor, Dept. of Aerospace Engineering.

were actively built into aircraft structures as a means of controlling aircraft with the most notable technique being the ingenious “wing warping” employed by the Wright brothers for roll control.¹ Since that time, a gradual progression in aircraft control systems has seen a shift from these compliant based techniques to the currently used and widely accepted techniques of strategically placed, small deflection, discrete control surfaces. As successful as these present methods have been over the last century, aircraft designers, faced with the challenging needs of 21st century air forces, must now confront challenges that only a radical re-think in current aircraft design thinking can hope to overcome. Paramount to these challenges is the requirement for any future flight vehicle to possess the ability to perform and execute multiple, dissimilar mission roles and objectives. These can include a dual low subsonic and supersonic flight speed capability, extraordinary agility and control authority, and perhaps most importantly, an advanced stealth capability.

Some of the more recent morphing wing/aircraft concepts have dealt with aspects of flight control and/or multiple mission adaptability.²⁻⁹ Unfortunately however, many of these concepts were not pursued further or remain immature. Traditionally, morphing for flight control involves small, continuous adjustments in the shape of the wing³⁻⁵ and/or surrounding flowfield⁶ to manoeuvre the aircraft during flight. Morphing for mission adaptation however involves making larger shape changes in order to optimize, in flight, the wing characteristics for the current flight condition.⁷⁻⁹ In this paper, we take the view of large scale morphing for control, investigating a concept using independently controllable, articulated, split wingtips on a flying wing model to achieve basic manoeuvres. Using variable dihedral angle wingtips in this regard disrupts significantly the spanwise wing-loading symmetry, resulting in, conceivably, a more efficient method of lateral/directional control than through the articulation of discrete control surfaces into the mainstream.

The present concept is in fact a refinement of a previously-investigated concept,¹⁰ where the tips of a flying wing were folded symmetrically or unsymmetrically to achieve longitudinal and/or lateral/directional control. Though it appeared to be effective, a single pair of folding wingtips could not substitute for all the conventional control surfaces at the same time if one wanted to obtain a full control envelope: in particular, to perform level turns at arbitrary bank angles, the wingtip deflection needed to be combined with some elevator to trim the aircraft. The present concept is thus an attempt to control the wing solely with folding wingtips, removing the elevator from the control line by using a second pair of folding wingtips instead (see Fig. 1). With four independent multi-axis effectors, the system is then over-actuated, leading to some redundancy in the flight control system, which could be exploited to optimize secondary objectives (e.g. minimum drag, minimum bending moment) at fixed lift and moments.

II. Characteristics of the Investigated Airframe

A. Geometry

The model used for experimental testing was constructed of a blue foam core with a carbon fibre skin. The unmodified baseline configuration consisted of a planar trapezoidal wing with 30° LE sweep, with aspect and taper ratios of 4.6 and 0.56 respectively. The wing was untwisted and lofted with a 12% thick Zagi airfoil section with reflexed TE. Modifications to this baseline configuration were primarily performed at the tips through the addition of servo driven articulated hinges where the split wingtips were fixed. The assembly of the wing/wingtip interface conserved the sweep angle for the fore wingtips with the aft wingtip pair swept at an additional 7 deg. A schematic of the experimental wing model is shown in Fig. 1. The articulated wingtips (also referred to as winglets in the paper – we use both terms interchangeably) were untwisted and lofted with NACA 4412 airfoils, with the rear ones turned upside down (i.e. with negative camber, see Fig. 2). This particular arrangement is not arbitrary but comes from a numerical parametric study with the vortex lattice method presented in III.A. The goal of that preliminary analysis was to find a suitable arrangement of airfoil camber for the wingtips so that they could provide substantial roll and pitch moments given the prescribed control allocation scheme (described below).

B. Control Allocation Scheme

As mentioned in the introduction, with four control effectors and only three moments to control, the system is over-actuated. To keep things simple during our first analysis of the concept, it has been decided to actuate the rear winglets in tandem; thus the number of control lines is reduced by one (i.e. no more over-actuation). The following control allocation scheme is then prescribed: The rear winglets are always deflected symmetrically, acting as the primary pitch effector, while each front winglet can be deflected independently

of the others, acting primarily as a roll/yaw effector.

III. Analysis Tools

A. Numerical Method

To provide performance and stability estimates (for design purposes), we rely on a vortex lattice representation of the wing (the so-called vortex lattice method – VLM): in that linearized, potential flow model, angle of attack and sideslip are assumed to be small and the lifting surfaces and their trailing wakes are modeled as a discrete set of horseshoe vortex filaments stacked along the span and chord axes. The spanwise and chordwise loading is computed by solving a system of linear equations that enforce a flow-tangency condition at specified control points on the wing (the centroid of each bound ring-vortex). All the horseshoe vortices belonging to the same spanwise strip are co-planar, so the sectional camber is modeled by tilting the normal vector at the control point when applying the flow-tangency boundary condition (thin profile approximation). The forces and moments are obtained from the solved load distribution by applying the Kutta-Joukowski theorem. Provided that the dimensionless roll rates and reduced frequencies are slow enough, this steady-state aerodynamic model can be used to predict the instantaneous performance (viscous drag aside) and quasi-static stability derivatives during a rotary or oscillatory motion of the wing.

With regard to the articulated wingtips, the corresponding control derivatives are obtained from finite differences by perturbing the aerodynamic grid. Otherwise, stability derivatives are computed from a differentiated form of the Kutta-Joukowski theorem (the vortex strength sensitivities stemming from the differentiation are estimated by solving the linear system for unit rotation and translation velocities).

To extend the method to compressible flows (purely subsonic though), the Prandtl-Glauert similarity rule is applied.

All the computations were based on the following uniform discretization: 19 horseshoe vortices along the span of each winglet, and 7 along its chord; 50 horseshoe vortices along each semi-span of the baseline wing, and 14 along its chord.

B. Experimental Method

The model was installed inside the closed test section ($2.1\text{m} \times 1.5\text{m}$, see Fig. 3) of a closed circuit wind tunnel whose maximum operating freestream velocity was 60 m/s. The model was investigated at a flow speed of $20 (\pm 0.5)$ m/s, giving a Reynolds number of 3.18×10^5 based on the mean aerodynamic chord of the planar configuration. Analysed configurations included symmetric deflections of the aft wingtips and unsymmetric deflections of the fore wingtips, for angles of attack ranging from -4° to 16° (w.r.t the wing-root chord line). The model was mounted at mid-height in the test section, on top of a support strut connecting the model to a high-frequency, dynamic load cell mounted to the underside of the floor of the test section. The freestream turbulence level at the model station was approximately 0.2%. Access to the wind tunnel test section for the support strut was provided by a cutout in the wind tunnel floor which was covered, during wind tunnel testing, by two thin sheets of fibreboard. Each sheet was constructed to ensure no contact between the supporting strut and the test section was possible. Four high-tension wires were also installed between the active balance plate and the top of the support strut to increase the stiffness of the entire support system, thereby improving the natural frequency characteristics of the combination.

Forces and moments were acquired with a six axis balance (AMTI MC3A-500). The maximum lift, drag and side force capabilities of the cell were $\pm 2\text{kN}$, $\pm 1\text{kN}$, and $\pm 1\text{kN}$ respectively. Maximum range for the pitching moment, rolling moment and yawing moment were $\pm 56\text{Nm}$, $\pm 56\text{Nm}$, and $\pm 28\text{Nm}$ respectively. Assessment of the observed non-linearity as well as zero drift after a rigorous pre-testing preparation were found to be better than $\pm 0.5\%$. All data obtained from the load cell was digitised through a 16-bit dSpace data acquisition system, and all data taken over a period of approximately 30 seconds. Control surface position for each winglet was provided by directly coupled, precision potentiometers purposely built into the model.

All four servos (Digital Hitec HSR-5995TG) used to control the model were driven by a dSpace control system. This system was configured to generate pulse width modulated input signals (300 Hz) with variable duty cycles corresponding to a pulse width range of between $400\text{-}2100 \mu\text{s}$. Calibration of control surface position was carried out using a digital inclinometer (error $\pm 0.1^\circ$) positioned on the control surfaces and matched to a readout from the dSpace control system indicating the input signal pulse width. Achievable

dihedral angle magnitudes for the wingtips were -75° to $+75^\circ$ (positive dihedral is up wingtip, zero dihedral is in the wing plane). The same digital inclinometer was used to calibrate the angle of attack of the model which was measured relative to a flat, prefabricated cut-out at the mid-plane of the wing, co-incident with the chord line.

IV. Results and Discussion

In the results presented hereafter the following conventions apply:

- the reference area for all aerodynamic coefficients is the planform area of the fully planar configuration;
- the span of the planar configuration was used as reference length for the rolling and yawing moments;
- the mean aerodynamic chord of the unmodified, baseline trapezoidal wing was used as the reference length for the pitching moments;
- moments are given in the standard stability axes (x forward, y to the right of the pilot, z down) and taken positive according to the right-hand rule about those axes;
- moments are all referenced about the CG of the planar configuration, which can be assumed to be the CG of any of the non-planar configuration^a. The longitudinal position of the CG has been fixed at the foremost location of the aerodynamic centre (at about 73% of the wing root chord, as predicted by the VLM) so as to preserve the static longitudinal stability over the range of permitted wingtip dihedral angles.

A. Effect on performance

Deflecting the winglets off the wing plane, either symmetrically (aft wingtips) or unsymmetrically (fore wingtips) does not affect significantly the lift curves, as can be seen from Fig. 4 ($C_{L_{max}}$ remains about 0.8, and stall angle about 12°). It does however affect the aerodynamic efficiency (see Fig. 5) in the case of unsymmetric deflections of the front winglets at moderate angles of attack, with negative dihedral angle leading to better performance (roughly 10% improvement w.r.t. the configuration with both fore winglets in the wing plane). Deflecting one front winglet independently from the other, which remains in the wing plane, will create some roll (see section IV.B.2). Thus as far as aerodynamic efficiency is concerned a down winglet (negative dihedral angle) is the best option for creating roll.

B. Attainable moments and rates

1. Longitudinal control

Control of the longitudinal motion of the flying wing can supposedly be achieved by deflecting the aft winglets in tandem (changing then the effective area of the trimming surfaces), while the fore winglets remain fixed at a given dihedral angle, which we chose to be zero (i.e. in the wing plane). The observed pitching moments for such configurations are plotted versus the aft wingtip dihedral angle in Fig. 6. One can notice the presence of two monotonic segments in the pitching moment curve: one for negative dihedral angles, and the other for positive dihedral angles; both ranging from ± 30 to ± 75 . In those intervals, the pitching moment increases, almost linearly, with the magnitude (absolute value) of the dihedral angle. This indicates the feasibility of controlling the longitudinal attitude of the airframe: by setting both aft winglets at an intermediate dihedral angle in those intervals (say $\pm 50^\circ$, redesigning eventually the TE of the main wing so that the whole configuration is naturally trimmed at that intermediate dihedral angle), one can nose up (resp. down) the flying wing by increasing (resp. decreasing) at a fixed angle of attack the magnitude of the dihedral angle about this intermediate position. Similarly, if the angle of attack is allowed to change to accommodate to a new flight condition, decreasing (resp. increasing) the absolute amount of aft wingtip dihedral will trim the aircraft at a greater (resp. smaller) flight speed.

^asince wingtips are rotated about an axis parallel to the wing-root chord line, the chordwise location of the airframe CG remains unchanged during this transformation. Only its spanwise and vertical locations will change. However due to the small relative mass of the wingtips compared to the baseline wing, the spanwise and vertical shifts remain insignificant even in the case of a uniform mass distribution, and are less than 1% of the root chord. Therefore assuming the CG is the same for all the configurations is legitimate.

2. Lateral/directional control

With the aft winglets deflected in tandem at a given dihedral angle so as to trim the flying wing longitudinally, roll and yaw can be created by deflecting one of the fore winglets off the wing plane. Predicted and observed moments are shown in Figs. 7 to 9 for configurations with aft winglets set symmetrically at either -45° or 0° or $+45^\circ$, left fore winglet fixed in the wing plane, and right fore winglet deflected off the wing plane. All the moments are relative to the configuration with both front winglets in the wing plane.

As far as rolling moments are concerned (Fig. 7), the agreement between experimental and numerical data is fairly good, except for the configuration with aft winglets fixed in the wing plane, where the VLM predicts negative roll for negative dihedral angles in $[0^\circ, -50^\circ]$ whereas the experiment does not. As expected, a positive rolling control moment is produced, that is the wing will roll to the right (i.e. to the side where the front winglet is off the wing plane), whether the winglet is deflected up or down (however in the particular case with aft winglets in the wing plane, positive dihedral angles need to be greater than $40^\circ \sim 60^\circ$ for positive roll to be produced – negative roll is produced otherwise!). As far as yawing moments are concerned (Fig. 8), the agreement between experimental and numerical data is also fair. Upward deflection of the right front winglet creates positive yaw (i.e. proverse yaw with respect to the generated roll moment) and vice versa. This effect was expected since the side-force produced on the deflected fore winglet is acting inward, behind the CG. Therefore deflecting the front winglet upward from the wing plane is desired if one wants to achieve a coordinated turn with the 4-winglet control system. In terms of pitching moments (Fig. 9), the agreement between simulation and experiment is not as good as it was for roll and yaw, nevertheless numerical predictions reproduce the trend of the experimental data: a positive pitch is created (i.e. the flying wing will nose up) when the front winglet is deflected (enough) off the wing plane, which is a positive side-effect since it will help coordinate a turn when the wing is banked.

3. Improvement of the design

So far the wingtip airfoils of the analyzed configurations had zero incidence with respect to the main wing chord line (see Fig. 2). Pitch stiffness can be improved by tilting the aft wingtips forward, so that they have a nose-down attitude w.r.t the main wing. Similarly, the wingtip effectiveness in producing roll and/or yaw can be improved by tilting the fore wingtips backward so that they have a nose-up attitude w.r.t the main wing. To check this, configurations with a 5° positive incidence on the fore wingtips and/or a 5° negative incidence on the aft wingtips have been analyzed numerically and compared to their counterparts with zero incidence. Results in terms of reduced roll rates^b are shown in Fig. 10 for the configurations with aft winglets at $+45^\circ$. It can be seen from this figure that the positive incidence of the fore winglets increases the roll rate by about 20% at dihedral angles greater than 40° . With regard to the negative incidence of the aft winglets, one can also see that it has no significant influence on the roll rate.

The computed aft wingtip dihedral angles to trim the flying wing in straight flight at various lift coefficients (while both fore wingtips are planar) are shown in Fig. 11. Again the configuration with aft and fore winglets tilted apart is the most effective, allowing a wider range of lift coefficients in trimmed flight to be attained.

4. Comparison to wing-tip tilting

The effectiveness of the folding fore winglets with regard to rolling is assessed by comparing them to fixed-dihedral-angle, tiltable fore winglets (i.e. their incidence can be changed w.r.t the main wing). The predicted reduced roll rates for both roll control systems are shown in Fig. 12. One can immediately notice that the roll effectiveness of the folding winglet depends on the operating lift coefficient (the greater, the better) whereas for the tilting winglets, it does not. The range of incidence for the tilting wingtips has been limited to $\pm 10^\circ$ relative to the wing chord line because it can be safely assumed that outside this interval the tilted wingtips would be stalled and the roll effectiveness would decay. Besides, inside this interval, the VLM can be used to give a fair estimate of the maximum roll rate because attached flow prevails on the tilted lifting surfaces. The folding winglet does not suffer from this stall limitation, since deflecting the winglet off the wing plane

^bThe reduced roll rate was computed using the following formula: $\hat{p} = -C_{l_0}/C_{l_p}$, which is obtained from the equations governing the rotary motion of the wing by assuming one rotational degree of freedom and solving for the steady state. $\hat{p} = pb/2Vc_g$ is the dimensionless roll rate, C_{l_0} is the rolling moment that initiated the roll (rolling moment due to the rotation of the right fore winglet), and C_{l_p} is the damp-in-roll derivative about the state that initiated the roll. C_{l_0} and C_{l_p} were obtained on the basis of steady-state aerodynamics by using the VLM.

will decrease its effective angle of attack, diminishing therefore the risk of stall (that is why VLM predictions match experimental data quite well even for large deflections). Bearing all of this in mind, it appears that tilting wingtips are only superior to folding wingtips at low lift coefficients (for instance, at $C_L = 0.15$, maximum dimensionless roll rate is 0.05 for the tilting wingtips and 0.03 for the folding wingtips). Hence folding wingtips are more suitable at low speed for roll control.

5. Compressibility effects

The predicted trend of the maximum roll rate at fixed lift coefficient is plotted versus the Mach number in Fig. 13 (given the LE sweep angle of 30° , it is reasonable to assume the Prandtl-Glauert correction valid up to $Ma = 0.7$). It can be seen that the maximum roll rate decreases slightly with the Mach number, up to 10% at $C_L = 0.6$, and less for smaller lift coefficients.

C. Simulation of a level turn

The split-tip flying wing configuration was numerically analyzed in a turning airflow simulating a steady level turn governed by the following algebraic equations:

$$V_{cg} = \sqrt{2W/(\rho C_{L_0} S)} \quad (1)$$

$$C_L = C_{L_0} / \cos \phi \quad (2) \quad p = 0 \quad (5)$$

$$R = V_{cg}^2 / g \tan \phi \quad (3) \quad q = \Omega \sin \phi \quad (6)$$

$$\Omega = V_{cg} / R \quad (4) \quad r = \Omega \cos \phi \quad (7)$$

where C_{L_0} is the lift coefficient at zero bank angle, that is in straight level flight, upon initiation of the turn. Rotation rates were directly constrained through the prescribed bank angle and turn rate. The sideslip angle was fixed to zero. The control angles, γ_{LF} , γ_{RF} , γ_{Aft} , required to zero out the aerodynamic moments during the turn^c, as well as the angle of attack required to maintain the lift coefficient prescribed from Eq. (2), are obtained by solving the corresponding moment and lift equality constraint equations with Newton's method. The Newton step is obtained by solving the following linear system:

$$\begin{pmatrix} C_{L\alpha} & C_{L\gamma_{LF}} & C_{L\gamma_{RF}} & C_{L\gamma_{Aft}} \\ C_{l\alpha} & C_{l\gamma_{LF}} & C_{l\gamma_{RF}} & C_{l\gamma_{Aft}} \\ C_{m\alpha} & C_{m\gamma_{LF}} & C_{m\gamma_{RF}} & C_{m\gamma_{Aft}} \\ C_{n\alpha} & C_{n\gamma_{LF}} & C_{n\gamma_{RF}} & C_{n\gamma_{Aft}} \end{pmatrix} \begin{pmatrix} \Delta\alpha \\ \Delta\gamma_{LF} \\ \Delta\gamma_{RF} \\ \Delta\gamma_{Aft} \end{pmatrix} = \begin{pmatrix} C_L - C_L^* \\ -C_l^* \\ -C_m^* \\ -C_n^* \end{pmatrix} \quad (8)$$

The Δ 's symbolize the corrections to be added to the current guesses of angle of attack and control angles. The starred aerodynamic coefficients and the stability derivatives are evaluated at the current operating point (i.e. for the current guess of control angles and angle of attack). The system is updated until the Newton step becomes smaller than a prescribed tolerance. Converged results for C_{L_0} of 0.2 and 0.4 are plotted in Fig. 14 against the bank angle. Note that the fore winglets are always almost symmetrically deflected to trim the flying wing during the turn. Because the system of constraint equations is non-linear, there are multiple solutions^dsatisfying the constraints, as shown in Table 1; this allows for the optimization of a secondary objective function, such as minimum induced drag or minimum deflection, for instance. Results plotted in Fig. 14 have in fact been obtained by retaining among the multiple solutions only the combinations of dihedral angles leading to maximum span; such combinations should tend to minimize the induced drag during the turn.

V. Conclusion

A novel control method based on independently actuated, articulated split wingtips was investigated. Observed and predicted control moments about the 3 axes were in good agreement and demonstrated that

^cLimiting ourselves to the case of small turn rates (i.e. $b \ll 2R$), and assuming the thrust line passes through the aircraft CG, aerodynamic moments about the aircraft CG are zero to the first order in rotation rates.

^dThose multiple solutions were obtained by changing the initial guess of the control angles in Newton's method.

the proposed control effectors could generate proverse, multi-axis moments. In fact, multiple solutions exist to generate one set of control moments at a given flight point, which allows for the optimization of a second objective function, such as minimum drag for instance. It was also shown that the control system is more effective at moderate and high lift coefficients, so it could be applied to low speed morphing aircraft.




Acknowledgments

This work has been supported by a Marie-Curie excellence research grant funded by the European Commission.

References

- ¹Culick, F. E. C., "The Wright Brothers: First Aeronautical Engineers and Test Pilots," *AIAA Journal*, Vol. 41, No. 6, June 2003, pp. 985-1006.
- ²Jha, A. K., and KudvaSmart, J. N., "Morphing Aircraft Concepts, Classifications, and Challenges," Structures and Materials 2004: Industrial and Commercial Applications of Smart Structures Technologies, Proceedings of SPIE, Vol. 5388, pp. 213-224.
- ³Sanders, B., Eastep, F. E., and Forster, E., "Aerodynamic and Aeroelastic Characteristics of Wings with Conformal Control Surfaces for Morphing Aircraft," *Journal of Aircraft*, Vol. 40, No. 1, Jan.-Feb. 2003, pp. 94-99.
- ⁴Hall, J. M., "Executive Summary AFTI/F-111 Mission Adaptive Wing," WRDC-TR-89-2083, Sept. 1989.
- ⁵Khot, N. S., Zweber, J. V., Veley, D. E., Oz, H., and Eastep, F. E. "Flexible Composite Wing with Internal Actuation for Roll Maneuver," *Journal of Aircraft*, Vol. 39, No. 4, July-Aug. 2002, pp. 521-527.
- ⁶Natarajan, A., Kapania, R. K., and Inman, D. J., "Aeroelastic Optimization of Adaptive Bumps for Yaw Control," *Journal of Aircraft*, Vol. 41, No. 1, Jan.-Feb. 2004, pp175-185.
- ⁷Neal, D. A., Good, M. G., Johnston, C. O., Robertshaw, H. H., Mason, W. H., and Inman, D. J., "Design and Wind-Tunnel Analysis of a Fully Adaptive Aircraft Configuration," 45th AIAA/ASME/ASCE/AHS/ASC Structures, Structural Dynamics and Materials Conference, 19 – 22 April 2004, Palm Springs, California, AIAA 2004-1727.
- ⁸Bae, J., Seigler, T. M., Inman, D. J., and Lee, I., "Aerodynamic and Aeroelastic Considerations of A Variable-Span Morphing Wing," 45th AIAA/ASME/ASCE/AHS/ASC Structures, Structural Dynamics and Materials Conference, 19 – 22 April 2004, Palm Springs, California, AIAA 2004-1726.
- ⁹Henry, J. J., Blondeau J. E., and Pines, D. J., "Stability Analysis for UAVs with a Variable Aspect Ratio Wing," 46th AIAA/ASME/ASCE/AHS/ASC Structures, Structural Dynamics and Materials Conference, 18 – 21 April 2005, Austin, Texas, AIAA 2005-2044.
- ¹⁰Bourdin, P., Gatto, A., and Friswell, M. I., "The Application of Variable Cant Angle Winglets for Morphing Aircraft Control," 24th AIAA Applied Aerodynamics Conference, 5 – 8 June 2006, San Francisco, California, AIAA 2006-3660.

Table 1. Different combinations of wingtip dihedral angles trimming the flying wing at 30° bank angle for a flight speed of $V_{cg} = \sqrt{10W/(\rho S)}$.

Geometry	α (deg)	γ_{LF} (deg)	γ_{RF} (deg)	γ_{Aft} (deg)	C_{D_i}
	2.66	2.34	2.69	-41.60	0.0057
	2.77	-54.10	-53.81	68.41	0.0062
	3.62	169.80	169.66	142.99	0.0089

Zagi12 flying wing

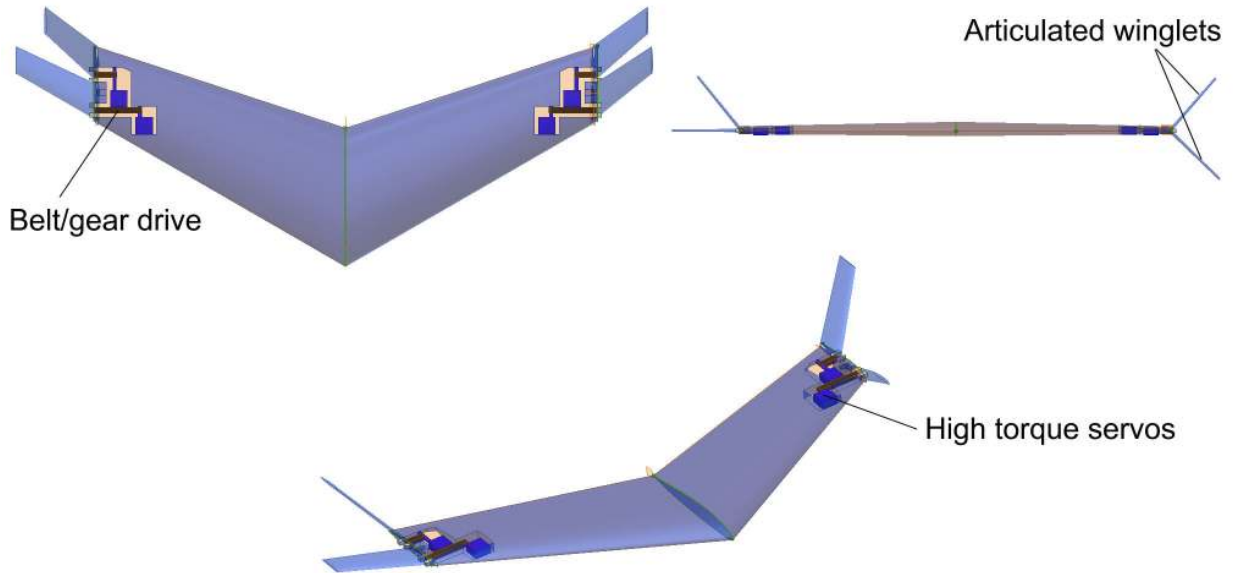


Figure 1. Wind-tunnel model and its internal structure.

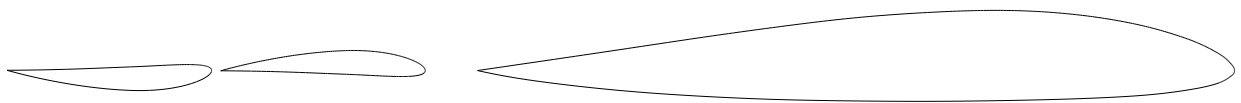


Figure 2. Butt-plane cuts at the wing root and the winglet root for the planar configuration, showing the airfoil sections (the airflow would come from the right).

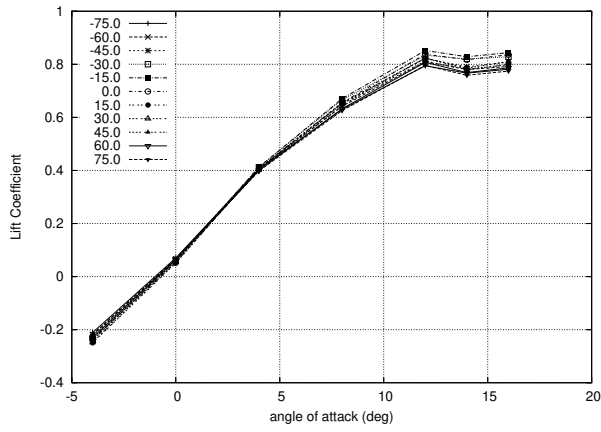


(a) Front view

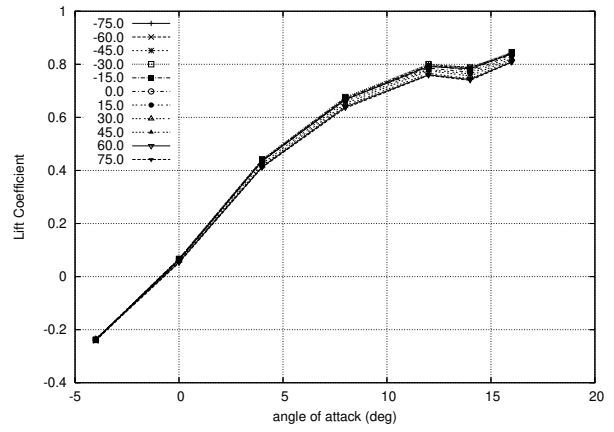


(b) Rear 3/4 view

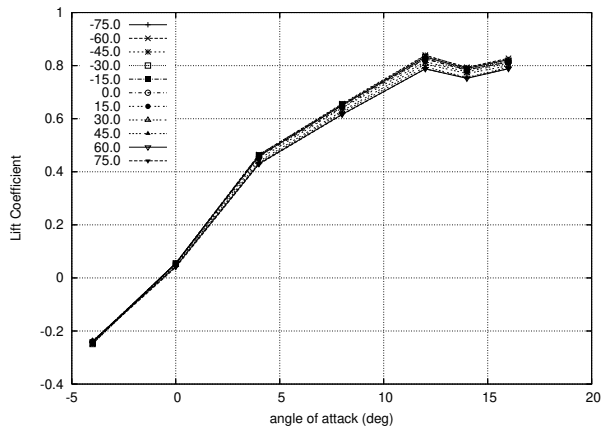
Figure 3. Experimental model as mounted in the wind-tunnel.



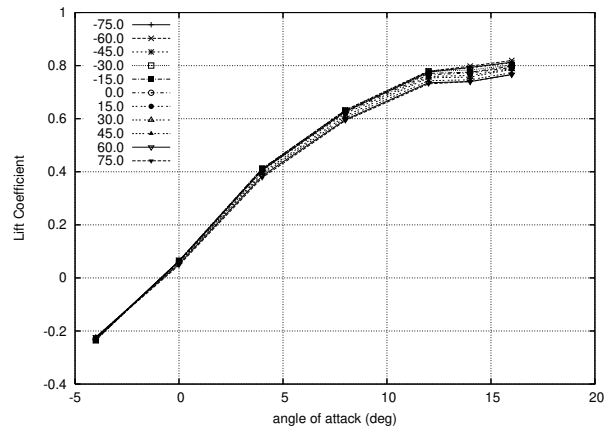
(a) Symmetric



(b) Unsymmetric -45

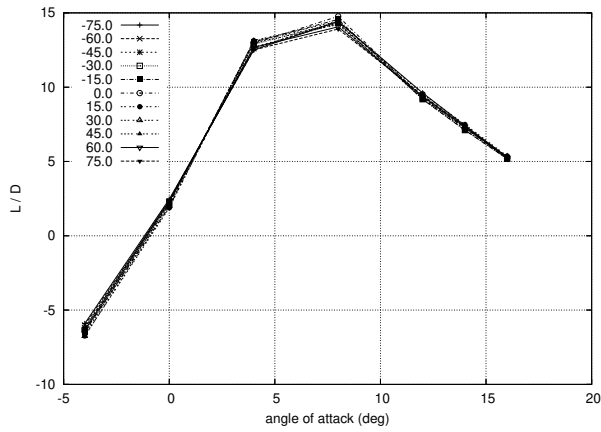


(c) Unsymmetric 00

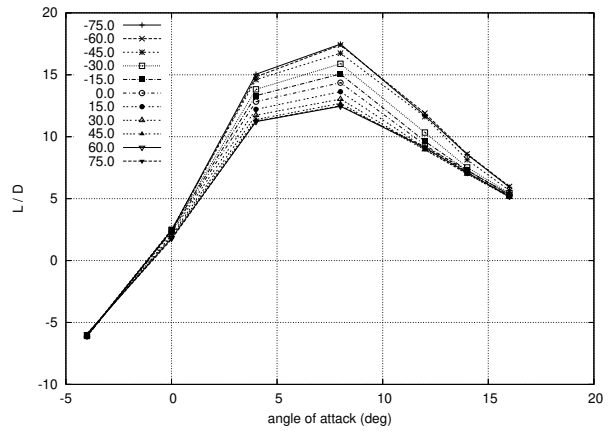


(d) Unsymmetric +45

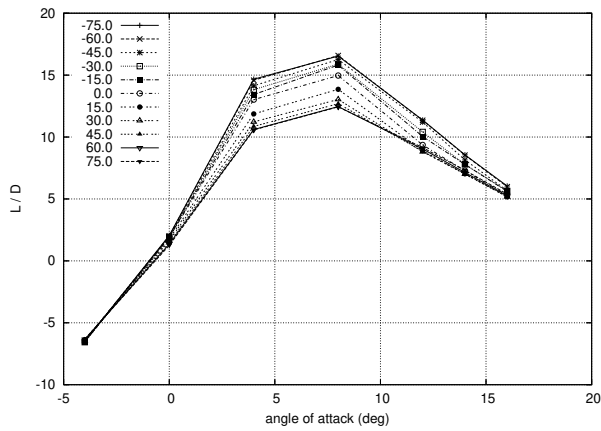
Figure 4. Lift curves from experimental data at $Re = 3.18 \times 10^5$. “Symmetric” refers to front winglets fixed in the wing plane and aft winglets deflected in tandem (the legends indicate aft winglet dihedral angle). “Unsymmetric [n]” refers to aft winglets fixed at [n]° dihedral angle, left front winglet fixed in the wing plane, and right front winglet deflected (the legends indicate right front winglet dihedral angle).



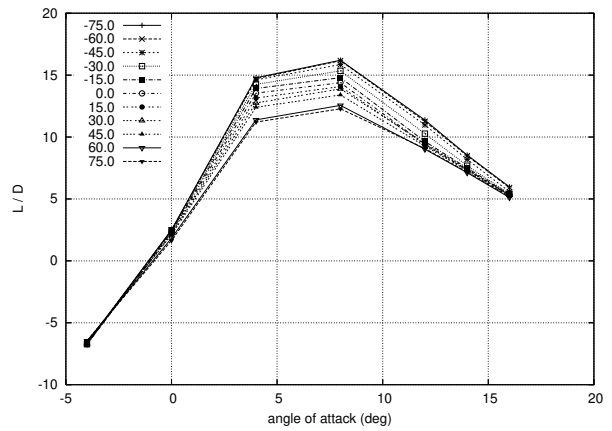
(a) Symmetric



(b) Unsymmetric -45



(c) Unsymmetric 00



(d) Unsymmetric +45

Figure 5. Lift to drag ratio from experimental data at $Re = 3.18 \times 10^5$. “Symmetric” refers to front winglets fixed in the wing plane and aft winglets deflected in tandem (the legends indicate aft winglet dihedral angle). “Unsymmetric [n]” refers to aft winglets fixed at [n]° dihedral angle, left front winglet fixed in the wing plane, and right front winglet deflected (the legends indicate right front winglet dihedral angle).

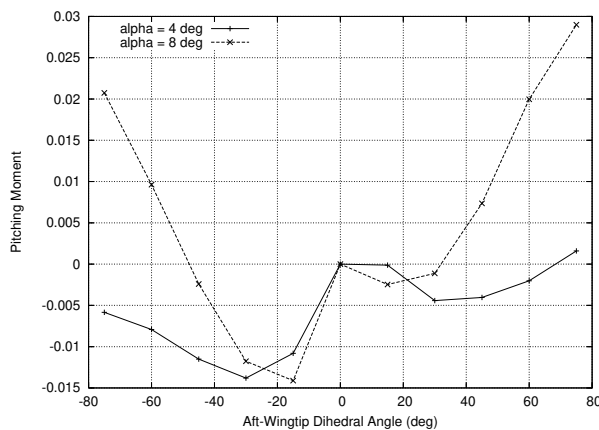
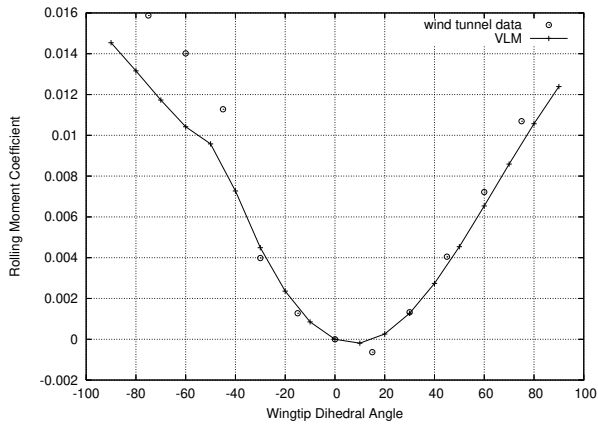
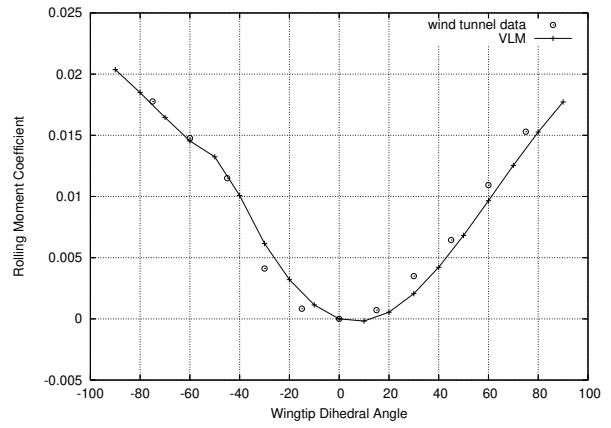


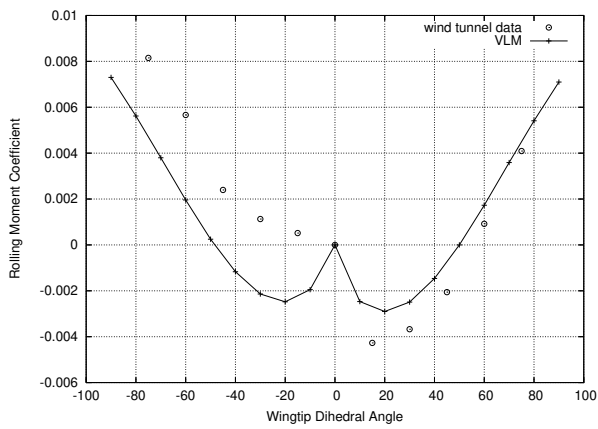
Figure 6. Attainable pitching moments from experimental data ($Re = 3.18 \times 10^5$) at 4° and 8° angle of attack with the fore wingtips fixed in the wing plane and the aft ones deflected in tandem. Moments are relative moments, with the fully planar configuration as reference.



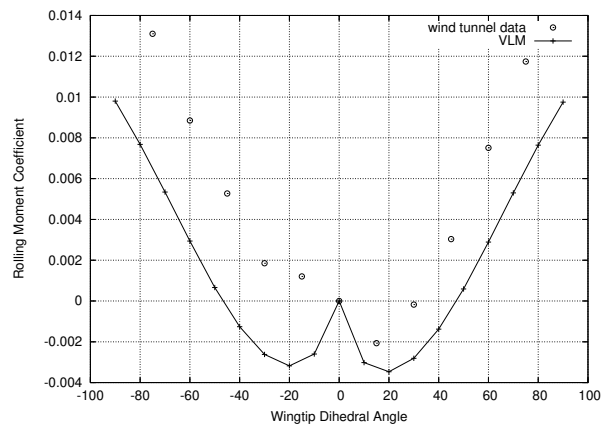
(a) Unsymmetric -45, $\alpha = 4$ deg



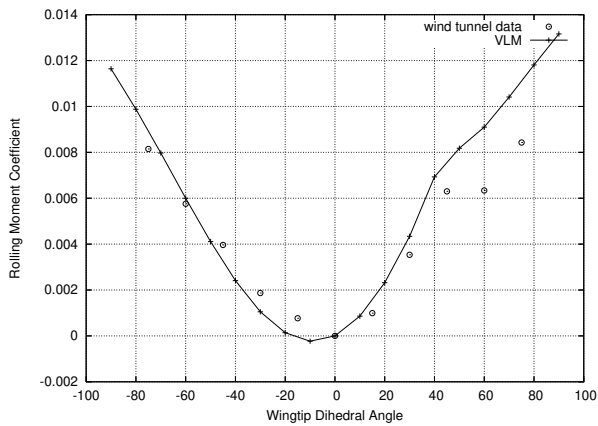
(b) Unsymmetric -45, $\alpha = 8$ deg



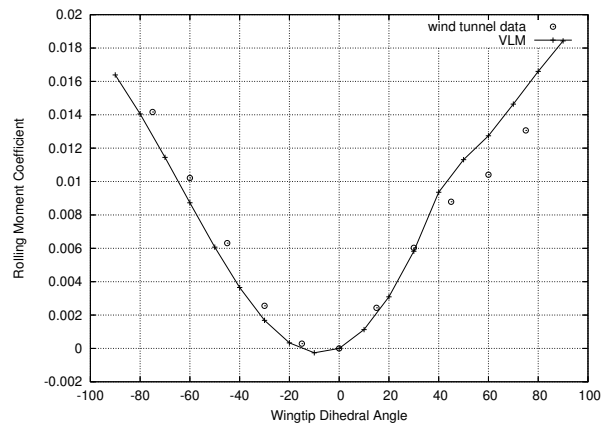
(c) Unsymmetric 00, $\alpha = 4$ deg



(d) Unsymmetric 00, $\alpha = 8$ deg

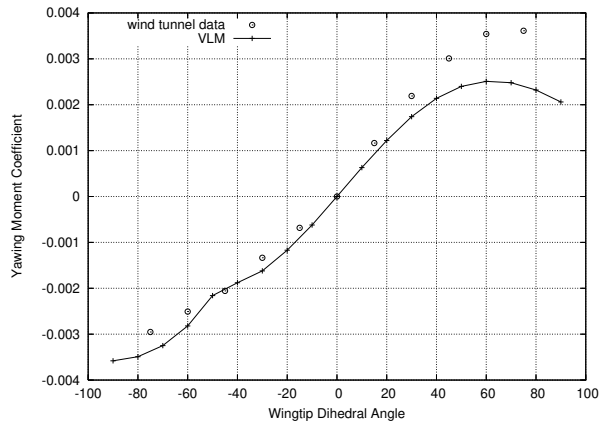


(e) Unsymmetric +45, $\alpha = 4$ deg

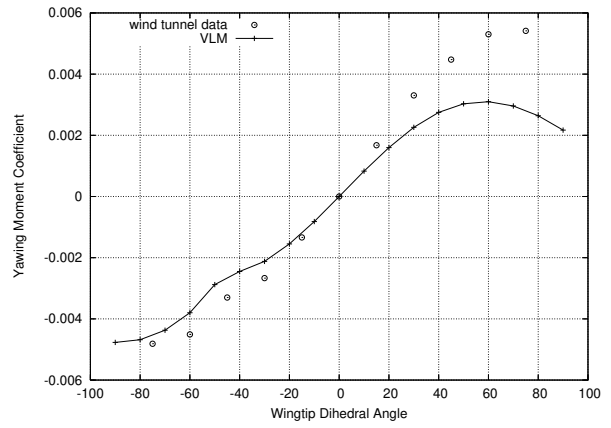


(f) Unsymmetric +45, $\alpha = 8$ deg

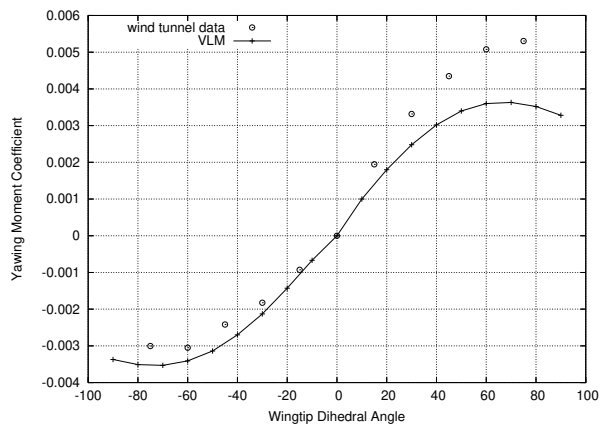
Figure 7. Attainable rolling moments from experimental data ($Re = 3.18 \times 10^5$) at 4° and 8° angle of attack when the right front wingtip dihedral angle is changed, while aft wingtips are set at a common dihedral angle and the left fore wingtip is in the wing plane. For comparison, numerical predictions (VLM) are also shown (the angle of attack for the VLM has been adjusted so that the observed and predicted lift coefficients match when both front winglets are undeflected).



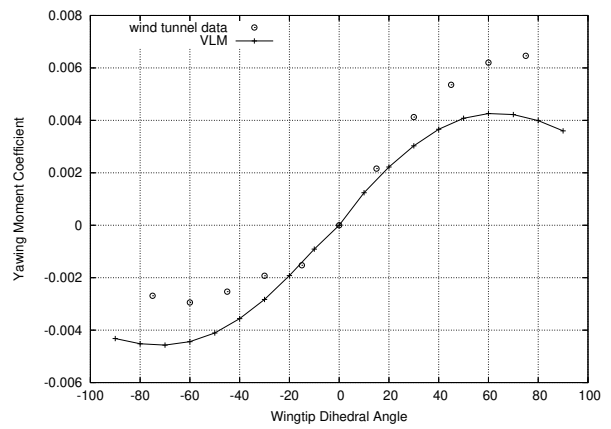
(a) Unsymmetric -45, $\alpha = 4$ deg



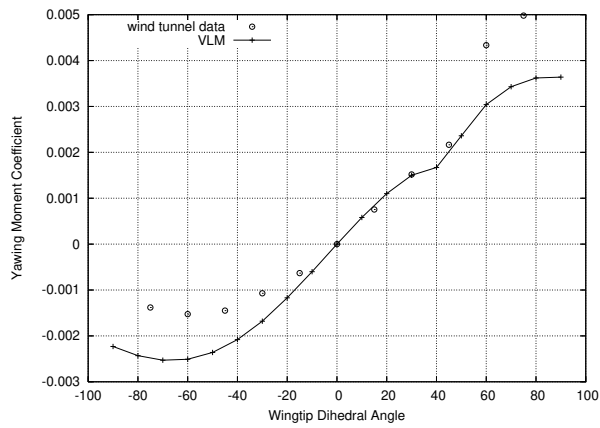
(b) Unsymmetric -45, $\alpha = 8$ deg



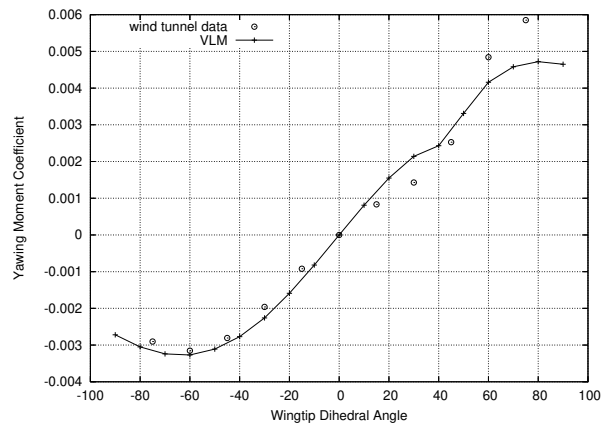
(c) Unsymmetric 00, $\alpha = 4$ deg



(d) Unsymmetric 00, $\alpha = 8$ deg

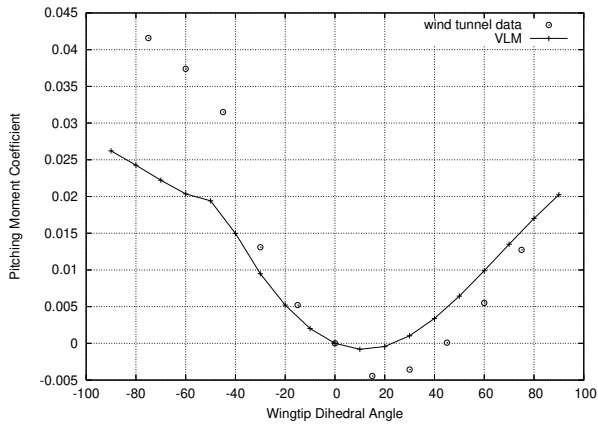


(e) Unsymmetric +45, $\alpha = 4$ deg

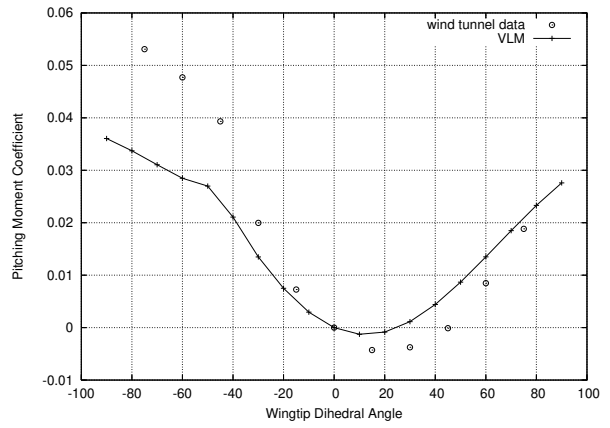


(f) Unsymmetric +45, $\alpha = 8$ deg

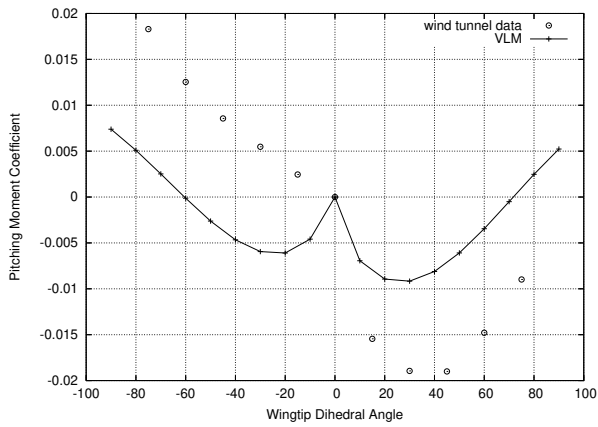
Figure 8. Attainable yawing moments from experimental data ($Re = 3.18 \times 10^5$) at 4° and 8° angle of attack when the right front wingtip dihedral angle is changed, while aft wingtips are set at a common dihedral angle and the left fore wingtip is in the wing plane. For comparison, numerical predictions (VLM) are also shown (the angle of attack for the VLM has been adjusted so that the observed and predicted lift coefficients match when both front winglets are undeflected).



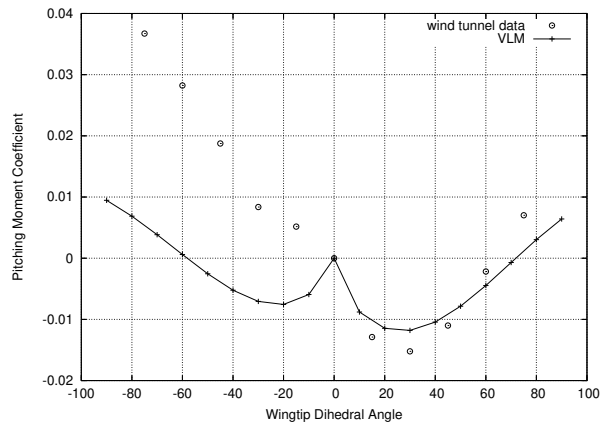
(a) Unsymmetric -45, $\alpha = 4$ deg



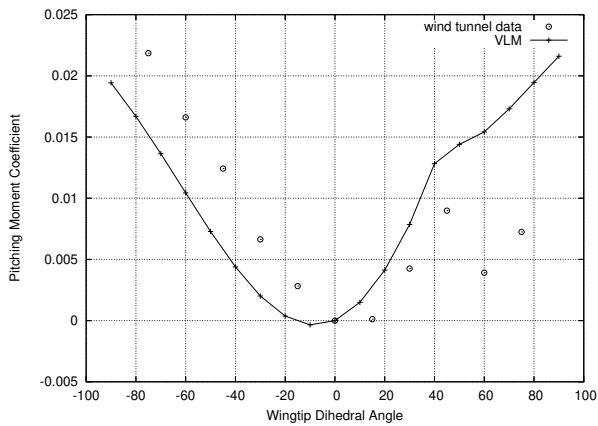
(b) Unsymmetric -45, $\alpha = 8$ deg



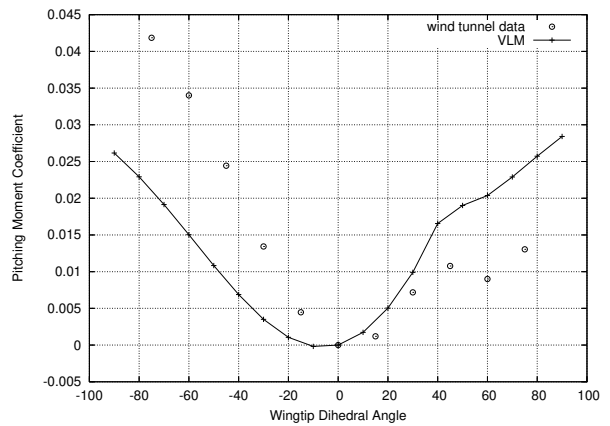
(c) Unsymmetric 00, $\alpha = 4$ deg



(d) Unsymmetric 00, $\alpha = 8$ deg



(e) Unsymmetric +45, $\alpha = 4$ deg



(f) Unsymmetric +45, $\alpha = 8$ deg

Figure 9. Attainable pitching moments from experimental data ($Re = 3.18 \times 10^5$) at 4° and 8° angle of attack when the right front wingtip dihedral angle is changed, while aft wingtips are set at a common dihedral angle and the left fore wingtip is in the wing plane. For comparison, numerical predictions (VLM) are also shown (the angle of attack for the VLM has been adjusted so that the observed and predicted lift coefficients match when both front winglets are undeflected). All moments are relative moments, with the fully planar configuration as reference.

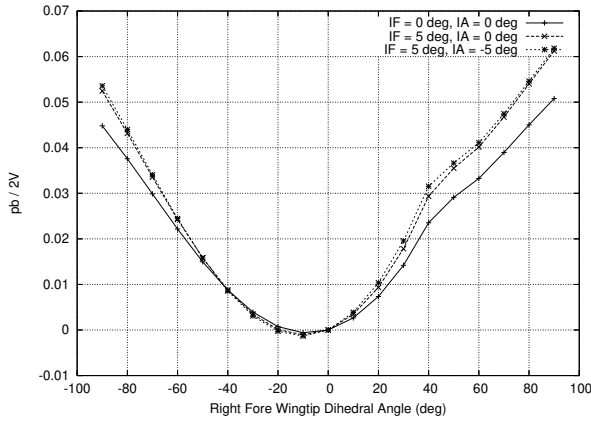


Figure 10. Effect of the winglet incidence on the steady-state roll rate (VLM predictions; $C_{L_0} = 0.6$; IF and IA refer respectively to the incidence of the fore and aft winglets).

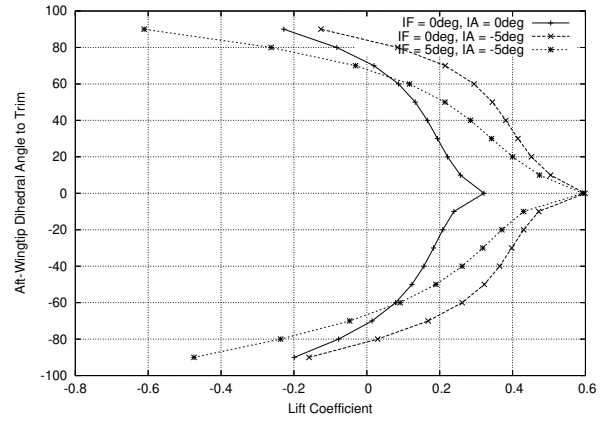
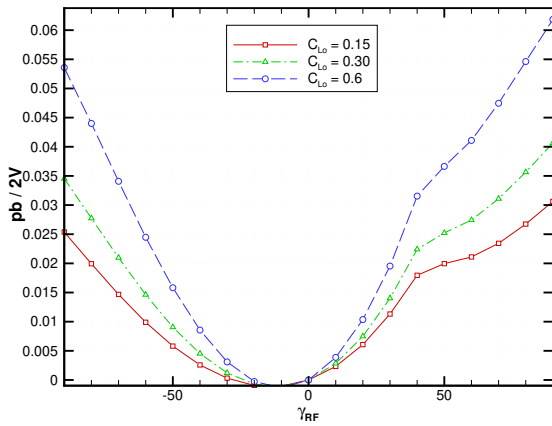
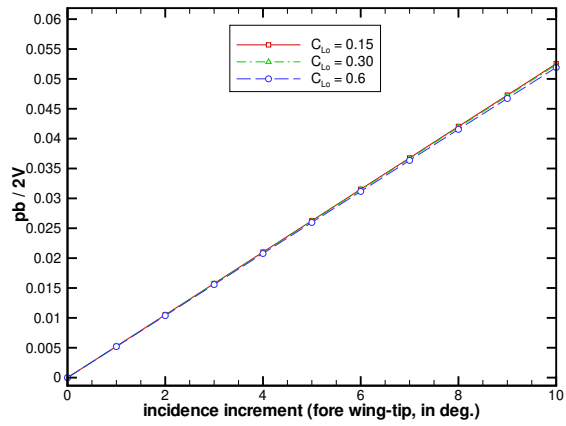


Figure 11. Aft-winglet dihedral angles to trim the flying wing longitudinally (VLM predictions; both fore winglets are fixed in the wing plane and aft winglets are symmetrically deflected; for each aft-winglet dihedral angle, the angle of attack was adjusted during the computation so as to zero out the pitching moment; IF and IA refer respectively to the incidence of the fore and aft winglets).



(a) Folding



(b) Tilting

Figure 12. Steady-state, dimensionless roll rates attainable by: (a) varying the right fore winglet dihedral angle, while the left one remains in the wing plane (incidence of both fore winglets is fixed at $+5^\circ$ w.r.t. wing chord); (b) varying the fore winglet incidence w.r.t. the wing chord (left and right winglets are tilted apart, with left one nosing up and right one nosing down). VLM predictions; in all cases aft winglets are fixed at $+45^\circ$ dihedral angle, with an incidence of -5° ; C_{L_0} refers to the lift coefficient of the configuration when both fore winglets are at zero dihedral angle (folding winglet case) or at zero incidence w.r.t. wing chord (tilting winglet case).

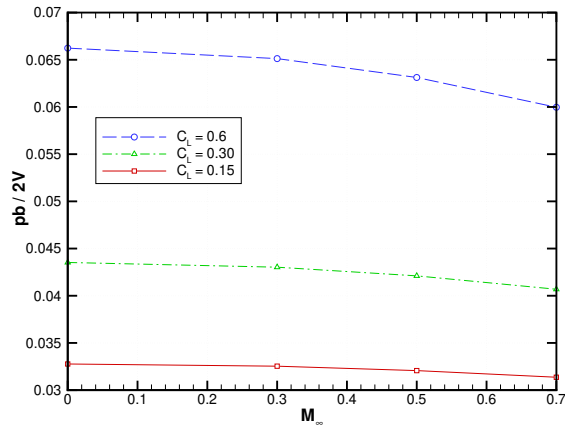


Figure 13. Predicted trend of the steady-state, dimensionless roll rate when the Mach number increases for the configuration with aft winglets set at 45° above the wing plane, left fore winglet in the wing plane, and right fore winglet upright at $+90^\circ$ dihedral angle.

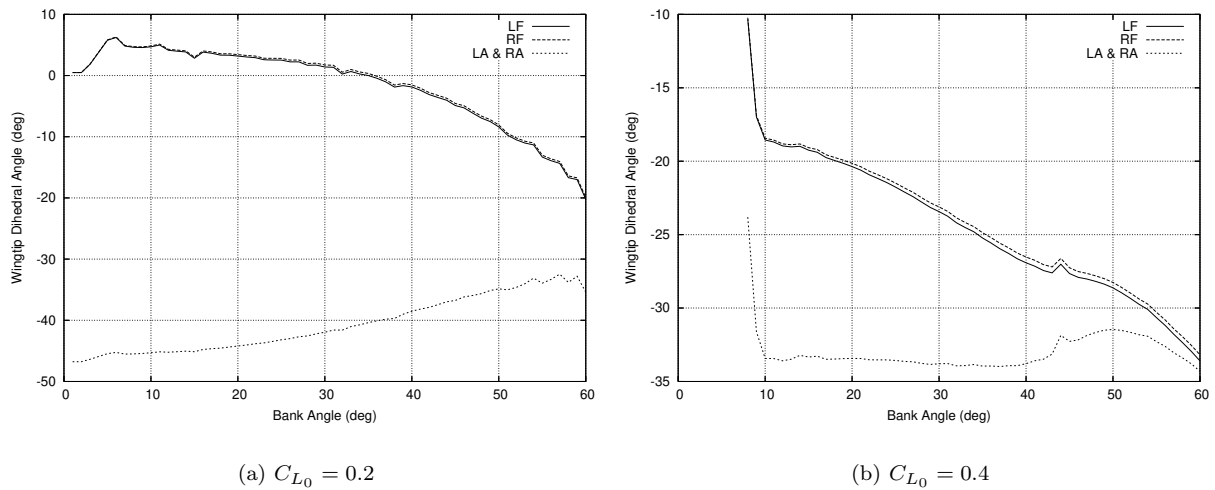


Figure 14. Control angles for the morphing flying wing to sustain a level turn at a given bank angle (VLM simulations; C_{L_0} is the lift coefficient upon initiation of the level turn from a straight, level flight). LF, RF, LA, and RA refer respectively to the Left Fore, Right Fore, Left Aft, and Right Aft winglet dihedral angles.